LHCb-CONF-2012-034
January 15, 2013

# First analysis of the $p$Pb pilot run data with LHCb

The LHCb collaboration [†]

**Abstract**

A first analysis of the data taken during the proton-lead pilot run is presented. The data sample corresponds to an integrated luminosity of $L_{\rm int} = 0.93 \pm 0.05\,\mu{\rm b}^{-1}$. A first measurement of the inelastic $p$Pb cross-section at a nucleon-nucleon centre-of-mass energy $\sqrt{s_{NN}} = 5.02\,{\rm TeV}$, with at least one charged particle in the region $2.5 < \eta_{\rm CM} < 4.5$ and $p_{\rm T} > 0.2\,{\rm GeV}/c$, yields $\sigma_{\rm inel} = 2.09 \pm 0.12\,{\rm b}$, where the uncertainty is purely systematic. Clean signals of strange and charm flavour production are observed. In $p$Pb interactions the average multiplicity in the proton hemisphere is found to be about a factor two larger than in $pp$ interactions when extrapolating to the same nucleon-nucleon centre-of-mass energy.



[†]Conference report prepared for the MPI@LHC 2012 Workshop, CERN, Switzerland, 3-7 December 2012. Contact author: Michael Schmelling Michael.Schmelling@mpi-hd.mpg.de

# 1 Introduction

The design of the LHCb experiment is optimized for the study of heavy flavour decays. However, its forward coverage and excellent vertexing, tracking and particle identification capabilities also allow many measurements in the field of electroweak physics and QCD. Recently the physics scope has been widened to include studies of proton-ion collisions at the LHC.

The first measurements from the LHC proton-lead pilot at a nucleon-nucleon centre-of-mass energy $\sqrt{s_{NN}} = 5.02\,\text{TeV}$ are shown and compared to the same quantities from proton-proton collisions at $\sqrt{s_{pp}} = 8\,\text{TeV}$. Since hadronic cross-sections only show a mild energy dependence, a direct comparison already gives a qualitative impression of the properties of $p$Pb compared to $pp$ interactions. At the quantitative level the difference in centre-of-mass energies must be taken into account.

Since the momentum per nucleon in the beam scales with $Z/A$ it follows that the nucleon-nucleon centre-of-mass system in a proton-lead collision is boosted in rapidity $y$ by $\Delta y = 1/2 \ln A/Z \approx 0.46$ units in the direction of the proton. When comparing particle densities as a function of rapidity or pseudorapidity this shift needs to be taken into account. In the pilot run the proton direction was downstream from the vertex detector towards the muon system, i.e. while in $pp$ collisions the centre-of-mass pseudorapidity coverage of the LHCb tracking system is roughly from $2 < \eta_{\text{CM}} < 5$, it is $1.5 < \eta_{\text{CM}} < 4.5$ for $p$Pb collisions.

The pilot run was also used to test the LHCb SMOG system [1]. This allows neon to be injected into the LHCb interaction region, which increases the beam-gas interaction rate by two orders of magnitude and thus facilitates accurate measurements of the beam profile for a precise determination of the absolute luminosity. It also offers the possibility to perform fixed target physics with beam-gas interactions.

# 2 Detector and trigger description

The LHCb detector [2] is a single-arm forward spectrometer covering the pseudorapidity range $2 < \eta < 5$, designed for the study of particles containing $b$ or $c$ quarks. For the pilot run it was operated in its standard configuration. The detector includes a high precision tracking system consisting of a silicon-strip vertex detector (VELO) surrounding the $pp$ interaction region, a large-area silicon-strip detector located upstream of a dipole magnet with a bending power of about 4 Tm, and three stations of silicon-strip detectors and straw drift tubes placed downstream. The combined tracking system has a momentum resolution $\Delta p/p$ that varies from 0.4% at 5 GeV/$c$ to 0.6% at 100 GeV/$c$, and an impact parameter resolution of 20 µm for tracks with high transverse momentum. Charged hadrons are identified using two ring-imaging Cherenkov detectors. Photon, electron and neutral hadron candidates are identified by a calorimeter system consisting of scintillating-pad and preshower detectors, an electromagnetic calorimeter and a hadronic calorimeter. Muons are identified by a system composed of alternating layers of iron and multiwire proportional chambers. The trigger [3] consists of a hardware stage, based on information from the

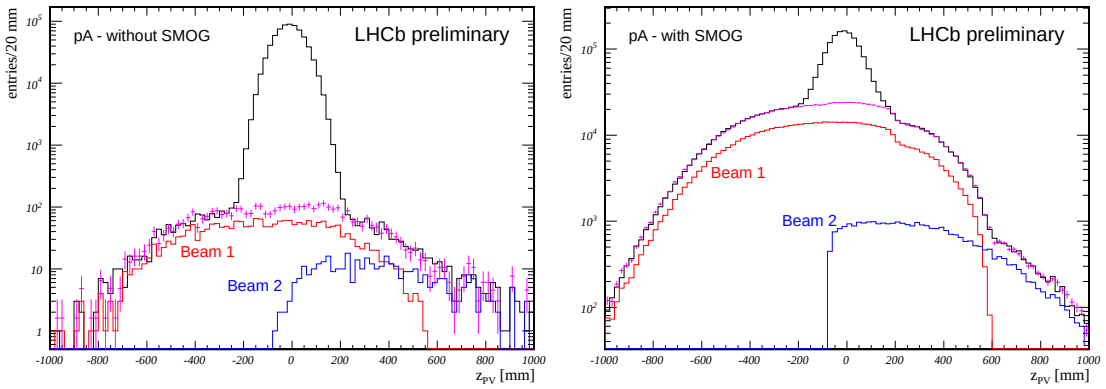


Figure 1: Distribution of the $z_{\rm PV}$ positions of reconstructed primary vertices in $p$Pb collisions without (left) and with (right) activated SMOG system. The distributions for only beam 1 (proton) and beam 2 (lead) are shown in red and blue, respectively. The magenta points are the weighted sums of the two, with weights adjusted to reproduce the integrals over the $p$Pb distributions for $|z_{\rm PV}| > 300\,$mm.

calorimeter and muon systems, followed by a software stage which applies a full event reconstruction.

A low bias trigger was used during the $p$Pb pilot run to veto empty events. In addition, no-bias triggers (random sampling) were recorded at a high rate in order to collect as much monitoring information as possible. Using those events, the low bias trigger efficiency was determined to be 99% for events with at least one reconstructed good track. The efficiency is about 100% when two tracks are present.

# 3 Data sets and integrated luminosity

The determination of the integrated luminosity for the $p$Pb pilot run is described in Reference [4]. For the data with (without) the SMOG system the integrated luminosity is $0.569\,\mu{\rm b}^{-1}$ ($0.361\,\mu{\rm b}^{-1}$). The statistical uncertainties of those numbers are negligible, the systematic uncertainty is estimated as 5.2%.

In the analysis presented below, the $p$Pb data are compared to $pp$ data collected at a centre-of-mass energy of $\sqrt{s_{pp}} = 8\,$TeV. A sample of 1.2 million events recorded with a no-bias trigger and with a single reconstructed primary vertex (PV) has been selected from the high luminosity $pp$ data collected in summer 2012 and processed with the same version of the reconstruction program as the $p$Pb data. After beam-gas background subtraction (see section 4) the $p$Pb data contain 1.8 million events with a single PV.

Primary vertices must have at least five associated track segments in the VELO. Not all of those segments form actual tracks traversing the entire tracking system. When comparing $pp$ and $p$Pb data, only tracks with a track-fit $chi^2$ per degree of freedom $\chi^2/{\rm NDF} < 3$ are used in the analysis.

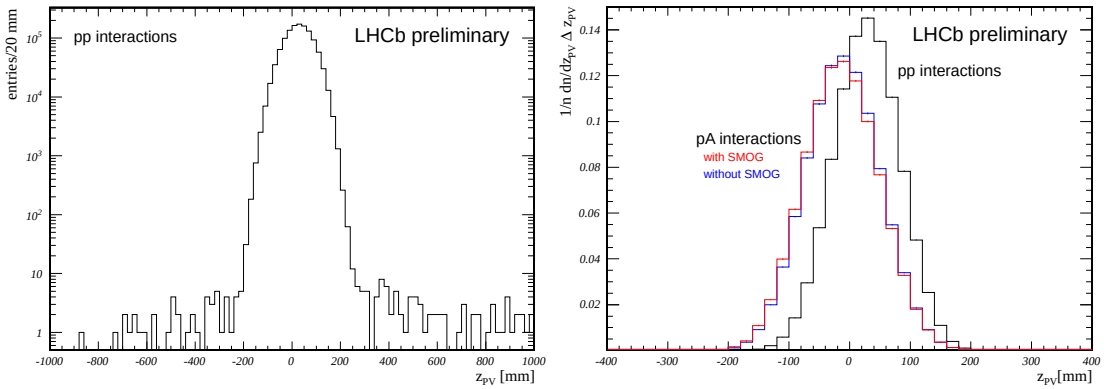


Figure 2: Distribution of the $z_{\rm PV}$ positions of reconstructed primary vertices in $pp$ collisions (left) and comparison of the luminous region between $pp$ and beam-gas-subtracted $p$Pb interactions (right). For comparison the histograms are normalised to unit area. The background subtracted $p$Pb data with SMOG are shown in red, the one without SMOG in blue.

# 4 Beam-gas subtraction

While background from beam-gas interactions is negligible for high luminosity $pp$ running, it constitutes a visible component for normal $p$Pb running and becomes a sizeable contribution when the SMOG system is activated. Since events were also recorded with only a single beam in the interaction region, the beam-gas background from either beam-1 (proton) or beam-2 (lead) could be measured from the distribution of the longitudinal position, $z_{\rm PV}$, of reconstructed primary vertices.[1] For any observable $x$ measured in bunch crossings with beam-1 only (BX1), beam-2 only (BX2) and beam-beam interactions (BX3), the background-subtracted results in beam-beam events then are determined by $x_{corr} = x(BX3) - a_1 x(BX1) - a_2 x(BX2)$. The weights $a_1$ and $a_2$ are the scaling factors for the distributions measured with BX1 and BX2 needed to reproduce the integral of the $z_{\rm PV}$-distribution for $|z_{\rm PV}| > 300\,$mm in BX3. The results are shown in Figs. 1 and 2. One clearly sees the different levels of beam gas background in the various samples, but also that beam-gas subtraction as described above works well for $p$Pb data with and without SMOG. After background subtraction the distributions for the two are in very good agreement, i.e. the subtraction works reliably for background levels which are different by two orders of magnitude. Although the luminous regions in $p$Pb and $pp$ are at slightly different $z$-coordinates, they both are restricted to the region $|z_{\rm PV}| < 200\,$mm.

[1] LHCb uses a right-handed coordinate system with the $z$-axis pointing along the beam direction from the VELO towards the muon system. The $y$-axis points upwards along the vertical. Rapidity and pseudorapidity are measured along, transverse momenta perpendicular to the $z$-direction.

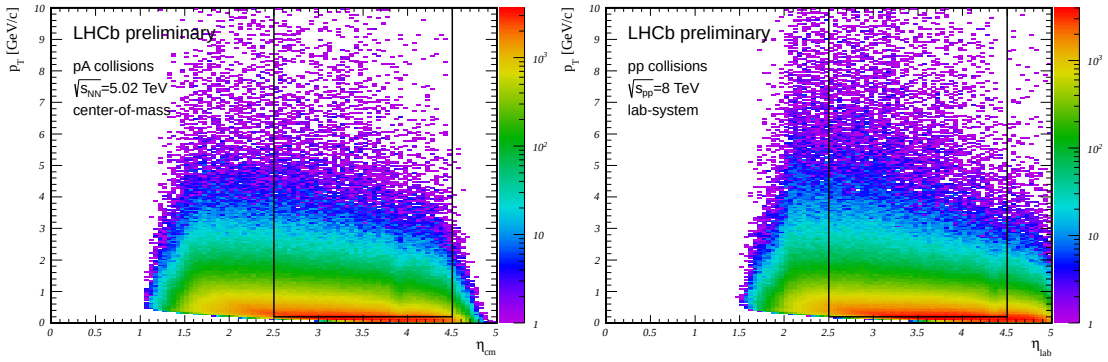


Figure 3: Transverse momentum versus pseudorapidity for charged particles originating from the luminous region. Distributions are shown for $p$Pb interactions in the centre-of-mass system (left) and for $pp$ collisions (right) in the laboratory frame, which is almost equivalent to the centre-of-mass frame. The boxes indicate the fiducial region used in the analysis.

# 5 Analysis strategy

Results will be given for particles in a kinematical region defined by cuts on transverse momentum $p_{\rm T}$ and rapidity $y_{\rm CM}$ or, for non identified particles, pseudorapidity $\eta_{\rm CM}$ along the $z$-direction in the nucleon-nucleon centre-of-mass system. In the second case the pion mass is assumed for the boost to the centre-of-mass system. The analysis is based on $p$Pb data recorded without SMOG. Data recorded with activated SMOG system are used as a cross-check.

Figure 3 illustrates the phase space coverage of the experiment and the effect of the Lorentz transformation from the lab to the centre-of-mass system. Transverse momentum versus pseudorapidity is shown for tracks originating from the luminous region. At the point of closest approach to the beam in the lab system, those tracks are required to have a transverse distance from the $z$-axis of less than 2 mm and a $z$-coordinate $|z| < 200$ mm. Also shown is the fiducial region used in the analysis, chosen such that it stays clear of the momentum cutoff of the tracking system induced by the spectrometer magnet, which is responsible for the phase space cut at low $p_{\rm T}$ and small pseudorapidity.

# 6 Inelastic $p$Pb cross-section

Having recorded at least one reconstructed track in the detector is sufficient to tag an event as inelastic $p$Pb interaction. With on average only approximately $1.5 \times 10^{-3}$ inelastic beam-beam interactions per bunch crossing, the pile-up is negligible for the data taken at the pilot run. If the integrated luminosity is known, simply counting events with at least one charged particle therefore allows the inelastic cross-section to be measured. In this analysis the inelastic proton-lead cross-section with at least one charged particle in the fiducial region $2.5 < \eta_{\rm CM} < 4.5$ and $p_{\rm T} > 0.2\,{\rm GeV}/c$ is determined.

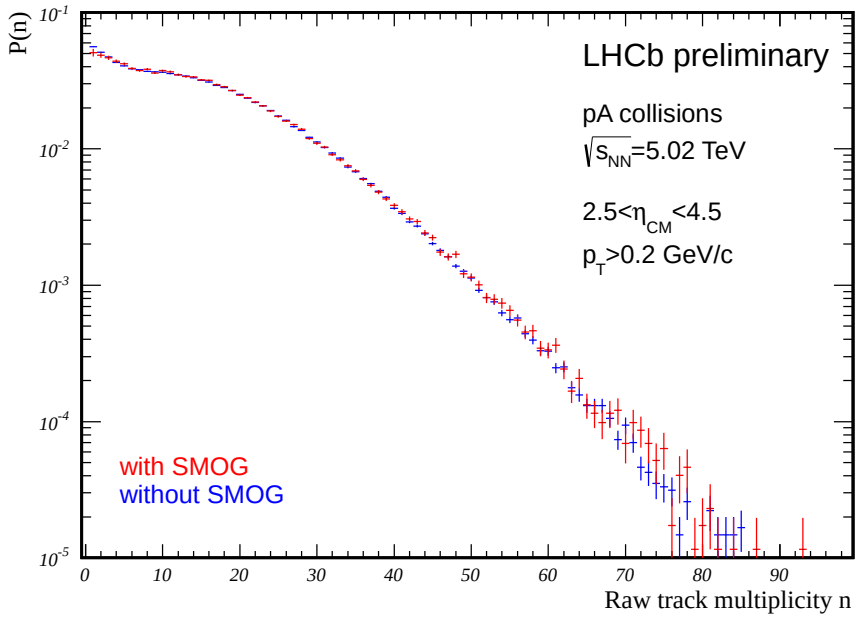


Figure 4: Probability distributions of uncorrected beam-gas subtracted track multiplicities in $2.5 < \eta_{\rm CM} < 4.5$ and $p_{\rm T} > 0.2\,{\rm GeV}/c$. The probability $P(n)$ to observe $n \geq 1$ tracks within the fiducial cuts is shown as a function of $n$. The multiplicity distributions for data taken with (red) and without (blue) the SMOG system in operation show good agreement after beam-gas subtraction.

The normalised beam-gas subtracted multiplicity distributions of tracks in the fiducial region is shown in Fig. 4, for events with and without the SMOG system in operation. Both are in good agreement. The event count for data taken without the SMOG system is $N_{\rm ev} = 738928 \pm 867$ which translates into raw cross-sections of $2.049 \pm 0.002 \pm 0.107\,{\rm b}$. The first uncertainty is the statistical uncertainty on the event count while the second one originates from the luminosity determination.

Spurious tracks from random hit combinations and multiply reconstructed particles do not affect the measurement of the event count since both are proportional to the number of charged particles in the event. Corrections which have to be considered are for the pile-up, the trigger and tracking efficiencies. Since during the pilot run the pile-up was below one permille [4] the corresponding correction is negligible. The trigger has an efficiency of 99% for single track events and is fully efficient for larger multiplicities. An efficiency of 100% is assumed, with a systematic uncertainty of 1%. The effect of smearing which moves particles with track parameters close to cut values in and out of the fiducial region, is negligible.

The dominant correction is for cases where tracks were emitted into the fiducial region, but as a consequence of the finite track finding efficiency of the spectrometer none was reconstructed. Since an event with $n$ tracks emitted in the fiducial region is not counted only if none of the tracks is reconstructed, the probability to keep the event is

$p_n = 1-(1-\varepsilon)^n$, with $\varepsilon$ the single track finding efficiency. For large values $n$ the probability $p_n$ quickly approaches unity even for values $\varepsilon \ll 1$. Estimating the event count probability $\varepsilon_{\rm ev}$ by folding $p_n$ with the measured raw measured multiplicity distribution $P(n)$, yields $\varepsilon_{\rm ev} = \sum_n p_n P(n) = 0.98 \pm 0.02$, where the uncertainty resulting from a rather generous variation $0.6 < \varepsilon < 1$ that covers also extreme cases of the track finding efficiency in the fiducial region, is purely systematic. Statistical uncertainties are completely negligible.

In principle, the measurement could also be affected by the small beam-crossing angle of approximately 0.3 mrad which leads to a small transverse boost, and the impact of a wrong mass assignment for a fraction of the tracks in the determination of $\eta_{\rm CM}$. It has been checked that the change in event count is less about 3% of the statistical uncertainty when assuming all particles to be massless and a crossing angle of 0.3 mrad.

The cross-section for inelastic $p$Pb collisions with at least one charged track in the range $2.5 < \eta_{\rm CM} < 4.5$ and $p_{\rm T} > 0.2\,{\rm GeV/c}$ becomes

$$\sigma_{\rm inel}(p{\rm Pb}, {\rm track}) = 2.09 \pm 0.12\,{\rm b}\ . \tag{1}$$

The total uncertainty is obtained by adding the individual contributions in quadrature. The statistical uncertainties are negligible, the systematics are dominated by the 5.2% incertitude on the luminosity measurement. Using the data taken with the SMOG system as a cross-check one finds a result perfectly consistent with (1), but, as a consequence of the large beam-gas background, with slightly larger uncertainties.

# 7 Multiplicities

To compare the track multiplicity in $pp$ and $p$Pb interactions, the tracks within the fiducial region are counted. In addition to coming from the luminous region, the tracks are required to have a track fit $\chi^2/{\rm NDF} < 3$. To assure approximately the same pile-up for the selected events, only events with a single reconstructed primary vertex are accepted. Since a primary vertex has at least five track segments in the VELO, the primary vertex requirement will slightly bias the low multiplicity region even though the VELO acceptance is significantly larger than the fiducial region used for the multiplicity measurement. For a comparison between $pp$ and $p$Pb, however, the effect is of secondary importance.

The preliminary uncorrected result, comparing $pp$ and $p$Pb interactions is shown in Fig. 5. One clearly sees a significantly enhanced multiplicity per event in $p$Pb compared to $pp$, the average number of tracks per event in $p$Pb interactions being approximately twice as large as in $pp$ interactions.

The measured multiplicities should be corrected for tracks from secondary interactions, multiply reconstructed tracks, spurious tracks from random combinations of hits, and for track finding efficiency. In the ratio many effects cancel, but residual differences are expected since the fiducial regions as defined in the centre-of-mass system correspond to different regions in the detector, and because the performance of the tracking system varies slightly with the track multiplicity. In addition a correction for different residual pileup in the selected event samples has to be applied and the different nucleon-nucleon

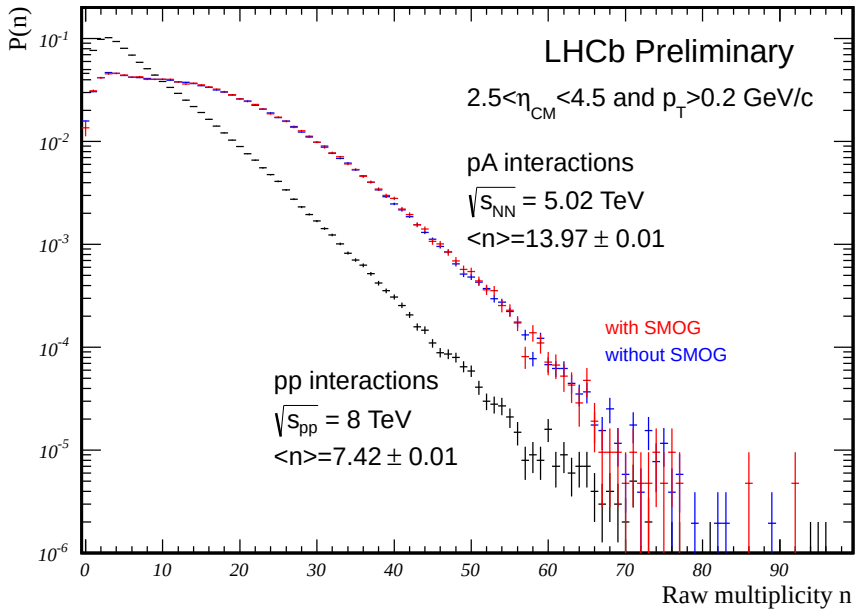


Figure 5: Probability distributions of uncorrected beam-gas subtracted track multiplicities of $pp$ (black) and $p$Pb interactions (red and blue) in $2.5 < \eta_{\rm CM} < 4.5$ and $p_{\rm T} > 0.2\,{\rm GeV}/c$. The probability $P(n)$ to observe $n$ tracks within the fiducial cuts is shown as a function of $n$. Only events with a single reconstructed primary vertex with at least five associated track segments contribute. The $p$Pb distributions are shown for data taken with (red) and without (blue) the SMOG system in operation.

centre-of-mass energies have to be accounted for. These corrections have not yet been applied. A first estimate of those effects suggests that the correction will increase the ratio of the average multiplicities $R_n = \langle n_{p\rm Pb}\rangle/\langle n_{pp}\rangle$ by about 10%.

# 8 Strangeness and charm production

In the following a first, uncorrected, comparison of flavour production in $p$Pb and $pp$ collisions is presented. Like for the case of the charged particle multiplicities, the comparison is performed in the nucleon-nucleon centre-of-mass system, in the fiducial region $2.5 < y_{\rm CM} < 4.5$ and $p_{\rm T} > 0.2\,{\rm GeV}/c$. Here, since the particle masses are known, rapidity is used instead of pseudorapidity and calculated with the PDG values of the particle masses. The analysis is based on events with a single reconstructed primary vertex. Since decay products from long-lived particles do not point back to the primary vertex, the requirement to originate from the luminous region is dropped for the daughter tracks.

The ratio $R(X) = Y(X)_{p\rm Pb}/Y(X)_{pp}$ of the yields $Y$ for particles of type $X$ per primary vertex between $p$Pb and $pp$ is used to illustrate the enhancement in particle production when going from $pp$ to $p$Pb. The same set of corrections as for the ratio $R_n$ of the average multiplicities would have to be applied to $R(X)$. Taking into account that two tracks

per decay are involved and that for the same kinematical region in the nucleon-nucleon centre-of-mass system more $V^0$ particles will decay outside of the acceptance in $p$Pb than in $pp$ interactions, one expects the $p$Pb/$pp$ ratio $R(X)$ to receive positive corrections between 7% and 16%.

## 8.1 Strangeness production

The most obvious signals to search for are $V^0$ decays which can be identified by using a simple geometrical selection. An analysis similar to the one performed in [5] was used which exploits purely geometrical information to reject combinatorial background, *i.e.* the selection of candidates is only based on the $V^0$-topology. Invariant mass distributions for specific decays are determined by assigning the charged pion or proton mass according to the type of signal one is looking for. The signal yield is estimated from the excess observed above a linear background.

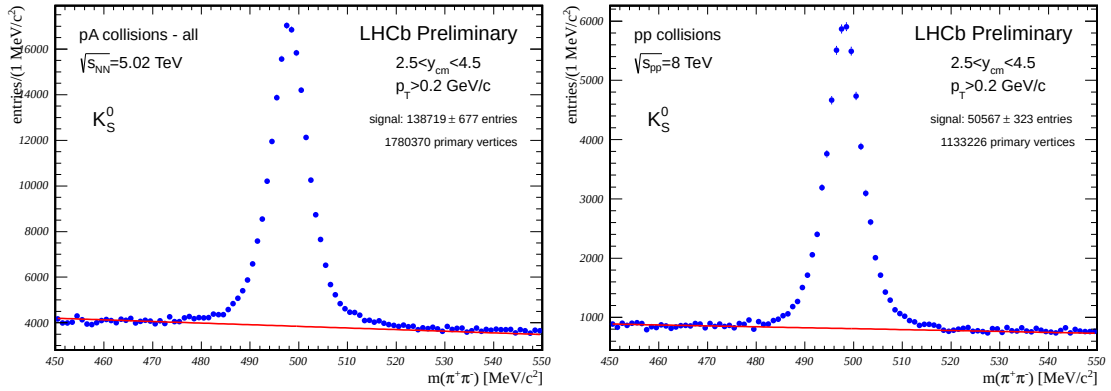


Figure 6: Production of $K^0_S$-mesons in $p$Pb collisions (left) and $pp$ collisions (right). The points are the experimental data, the red line indicates the assumed background.

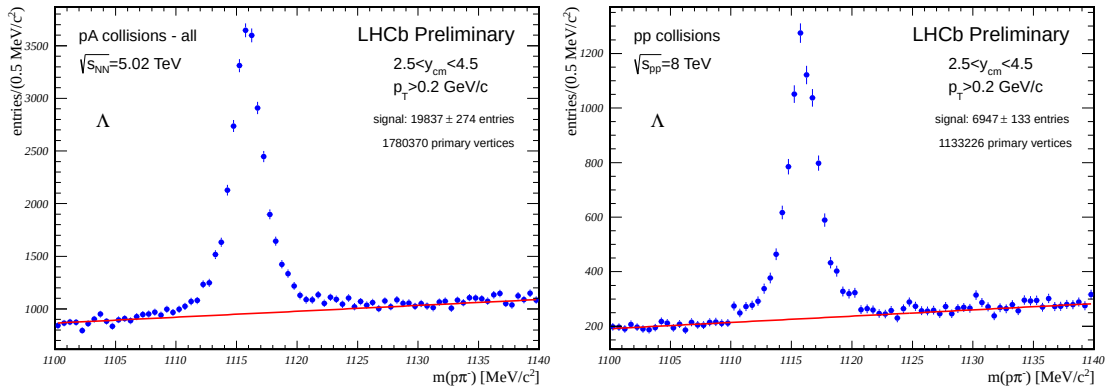


Figure 7: Production of $\Lambda$-hyperons in $p$Pb collisions (left) and $pp$ collisions (right). The points are the experimental data, the red line indicates the assumed background.

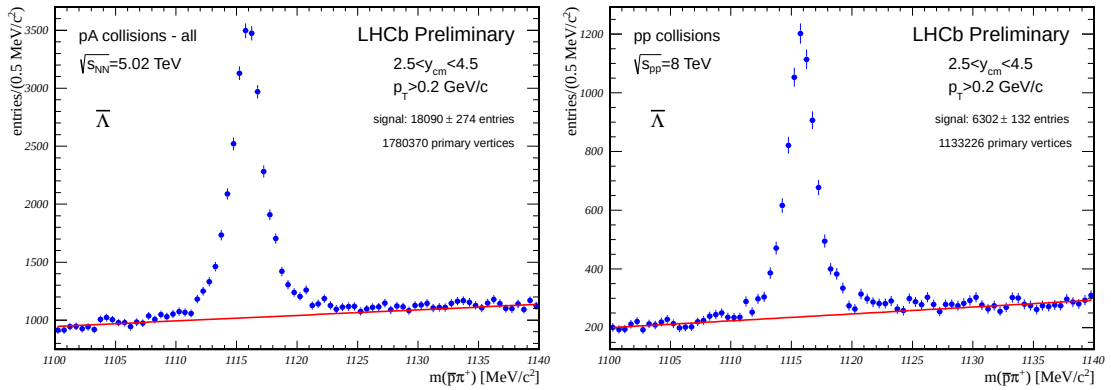


Figure 8: Production of $\bar{\Lambda}$-hyperons in $p$Pb collisions (left) and $pp$ collisions (right). The points are the experimental data, the red line indicates the assumed background.

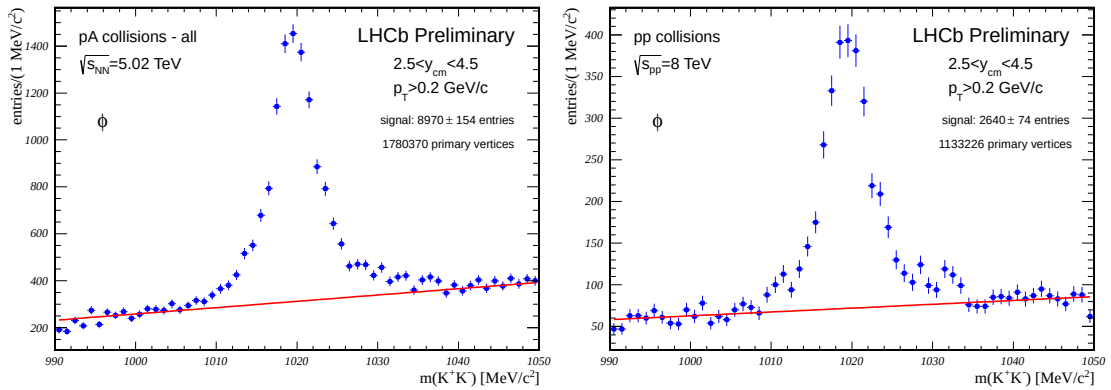


Figure 9: Production of $\phi$-mesons in $p$Pb collisions (left) and $pp$ collisions (right). The points are the experimental data, the red line indicates the assumed background.

Results for the $V^0$-decays in the channels $K^0_S \to \pi^+\pi^-$, $\Lambda \to p\pi^-$ and $\bar{\Lambda} \to \bar{p}\pi^+$ are shown in Figs. 6—8 in $p$Pb and $pp$ collisions. The uncorrected production ratios normalised to the number of primary vertices are $R(K^0_S) = 1.746 \pm 0.014$, $R(\Lambda) = 1.818 \pm 0.043$ and $R(\bar{\Lambda}) = 1.827 \pm 0.047$, the uncertainties being statistical only.

The measurement of $\phi$ meson production in the decay $\phi \to K^+K^-$ requires particle identification by the RICH. Asking for two well-identified opposite charge kaons with a distance of closest approach less than $100\,\mu$m is already sufficient to observe a clean signal. The resulting peaks for $p$Pb and $pp$ collisions are shown in Fig. 9. The $p$Pb/$pp$ production ratio normalised to the number of primary vertices is $R(\phi) = 2.163 \pm 0.071$. The uncertainty is purely statistical.

## 8.2 Charm production

Using RICH particle identification for the kaon and asking for a $V^0$-signature allows also $D^0 \to K\pi$ final states to be reconstructed. The sum over charge conjugate decays is shown

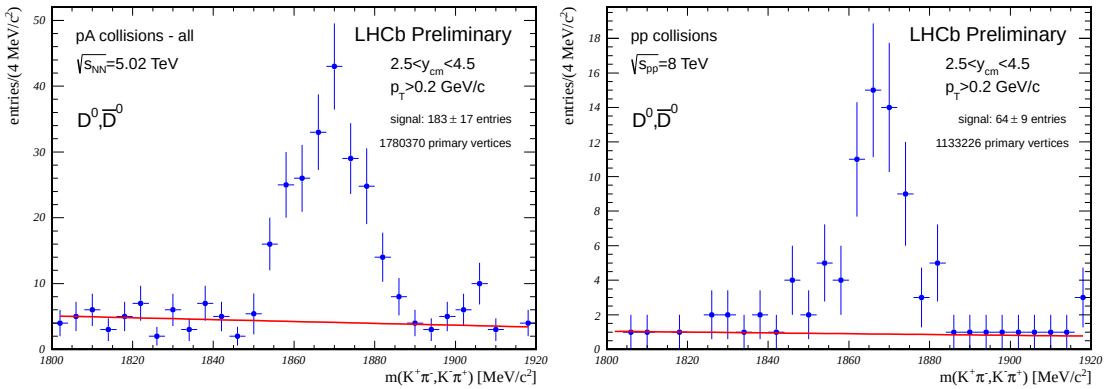


Figure 10: Production of $D^0$-mesons in $p$Pb collisions (left) and $pp$ collisions (right). The points are the experimental data, the red indicates the assumed background. Inclusion of charge conjugate modes is assumed.

in Fig. 10. The normalised $p$Pb/$pp$ production ratio is $R(D) = 1.820 \pm 0.307$, where the uncertainty is purely statistical.

A dedicated analysis using muon particle identification was performed to search for the decay $J/\psi \to \mu^+\mu^-$ in the $p$Pb data collected during the pilot run. A signal with a statistical significance close to four standard deviations is found and shown in Fig. 11. The data are fitted by a Crystal Ball function [6] for the signal and an exponential function for the background.

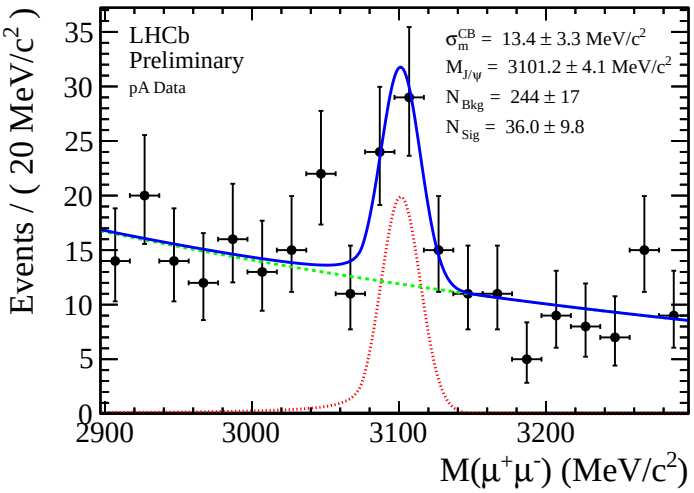


Figure 11: $J/\psi$-production in $p$Pb collisions. The points are the experimental data, the green curve shows the assumed background, and the red curve the Crystal Ball function used to describe the signal. The sum of signal and background is given by the blue line. Also indicated are signal and background yields, $N_{\rm Sig}$ and $N_{\rm Bkg}$, the fitted mass $M_{J/\psi}$ of the signal and the width $\sigma_{\rm m}^{\rm CB}$ of the gaussian part of the Crystal ball function.

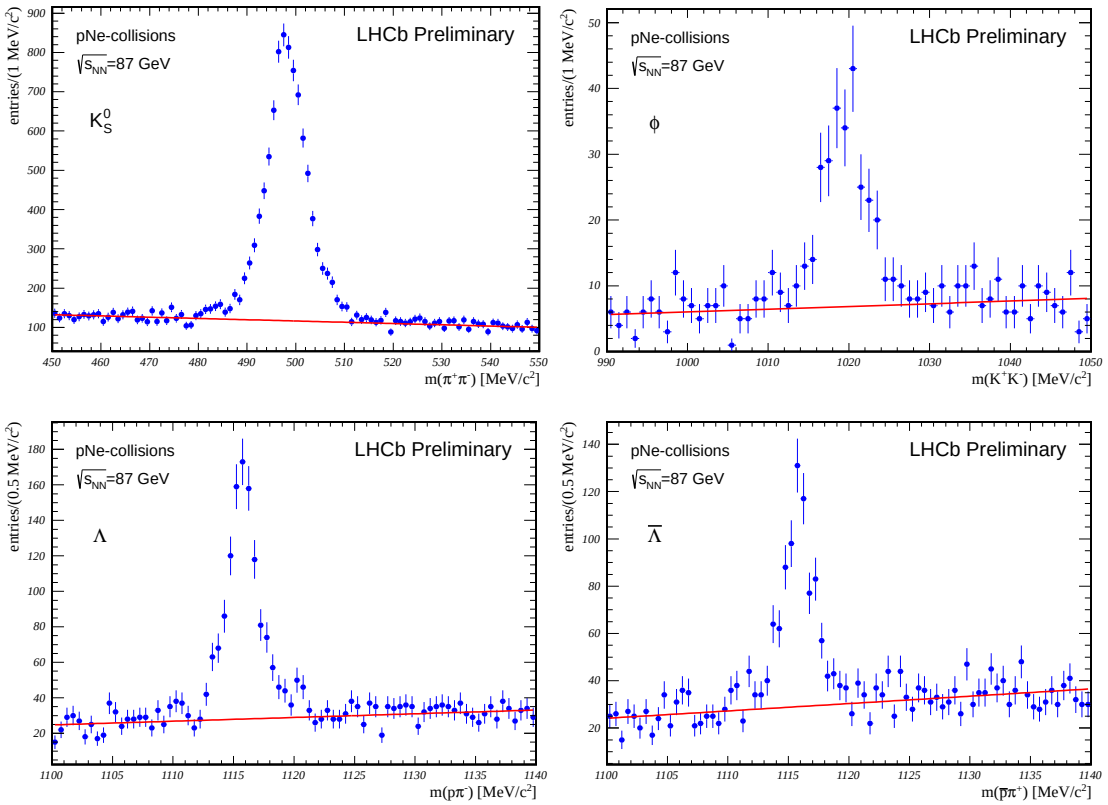


Figure 12: Fixed target production of strange particles, $K^0_s$ (top, left) and $\phi$ (top, right), and $\Lambda$ (bottom, left) and $\bar{\Lambda}$ (bottom, right), in pNe collisions. The points are the experimental data, the red indicates the assumed background.

# 9 Fixed target physics

Using the SMOG system, LHCb is in principle also able to perform fixed target physics. The rate of beam-gas interactions between the proton beam and the injected gas is sufficient to measure, for example, strangeness production in $p$Ne collisions. As shown in Fig. 12 clear signals are observed for strange mesons and baryons, respectively. In this case the nucleon-nucleon centre-of-mass energy is only $\sqrt{s_{NN}} = 87\,\text{GeV}$, and the whole system is boosted by $\Delta y \approx 4.5$ units in the direction of the proton beam. Viewed from the centre-of-mass of the collision, the LHCb detector thus measures the backward hemisphere.

# 10 Summary and conclusions

A first set of measurements on particle production in proton-ion collision based on the data taken during the $p$Pb run is presented. The available data set corresponds to an integrated luminosity of about $0.93\,\mu\text{b}^{-1}$. The data allow a first measurement of the inelastic $p$Pb cross-section at a nucleon-nucleon centre-of-mass energy $\sqrt{s_{NN}} = 5.02\,\text{TeV}$

with at least one charged particle in the region $2.5 < \eta_{\rm CM} < 4.5$ and $p_{\rm T} > 0.2\,{\rm GeV}/c$, giving $\sigma_{\rm inel} = 2.09 \pm 0.12\,{\rm b}$, with the uncertainty being fully systematic. The result is in good agreement with the expectation of scaling the visible $pp$ cross-section $\sigma_{{\rm vis},pp} = 59.1\,{\rm mb}$ [7] by $A^{2/3}$. Clean signals of strangeness and charm production are observed, even in beam-gas fixed target interactions. Comparing $pp$ and $p$Pb interactions, when going from $pp$ to $p$Pb one observes an increase of the average multiplicity by about a factor two in the proton hemisphere.

# Acknowledgements

We express our gratitude to our colleagues in the CERN accelerator departments for the excellent performance of the LHC. We thank the technical and administrative staff at the LHCb institutes. We acknowledge support from CERN and from the national agencies: CAPES, CNPq, FAPERJ and FINEP (Brazil); NSFC (China); CNRS/IN2P3 and Region Auvergne (France); BMBF, DFG, HGF and MPG (Germany); SFI (Ireland); INFN (Italy); FOM and NWO (The Netherlands); SCSR (Poland); ANCS/IFA (Romania); MinES, Rosatom, RFBR and NRC "Kurchatov Institute" (Russia); MinECo, XuntaGal and GENCAT (Spain); SNSF and SER (Switzerland); NAS Ukraine (Ukraine); STFC (United Kingdom); NSF (USA). We also acknowledge the support received from the ERC under FP7. The Tier1 computing centres are supported by IN2P3 (France), KIT and BMBF (Germany), INFN (Italy), NWO and SURF (The Netherlands), PIC (Spain), GridPP (United Kingdom). We are thankful for the computing resources put at our disposal by Yandex LLC (Russia), as well as to the communities behind the multiple open source software packages that we depend on.

# References

[1] C. Barschel, G. Schneider, *SMOG INSTALLATION PROCEDURE IN THE VELO ENVIRONMENT*, CERN EDMS Doc. Nr. 1166114, https://edms.cern.ch/document/1166114/1.

[2] LHCb collaboration, A. A. Alves Jr. *et al.*, *The LHCb detector at the LHC*, JINST 3 (2008) S08005.

[3] R. Aaij *et al.*, *The LHCb trigger and its performance*, `arXiv:1211.3055`.

[4] C. Barschel *et al.*, *Absolute luminosity measurement for the p-Pb pilot run*, in preparation.

[5] LHCb collaboration, R. Aaij *et al.*, *Prompt $K^0_S$ production in pp collisions at $\sqrt{s} = 0.9$ TeV*, Phys. Lett. **B693** (2010) 69, `arXiv:1008:3105`.

[6] T. Skwarnicki, *A study of the radiative cascade transitions between the Upsilon-prime and Upsilon resonances*, PhD Thesis, Institute of Nuclear Physics, Krakow, 1986, DESY-F31-86-02.

[7] LHCb collaboration, R. Aaij *et al.*, *Absolute luminosity measurement with the LHCb detector*, JINST **7** (2012) P01010, arXiv:1110:2866.